Title: Arousal state dependence of the cortical blood volume – pupil diameter relationship

Authors: Kevin L. Turner[1,2], Kyle W. Gheres[2,3], Patrick J. Drew*[1,2,3,4]

Affiliations:

[1]Department of Biomedical Engineering, The Pennsylvania State University, University Park, PA 16802

[2]Center for Neural Engineering, The Pennsylvania State University, University Park, PA 16802

[3]Department of Engineering Science and Mechanics, The Pennsylvania State University, University Park, PA 16802

[4]Departments of Biology and Neurosurgery, The Pennsylvania State University, University Park, PA 16802

***Corresponding author:** Patrick J. Drew - pjd17@psu.edu

Acknowledgements: This work was supported by NIH grants R01NS078168 and R01NS079737 to P.J.D.

Conflict of Interest: The authors declare no competing financial interests.

Author Contributions: K.L.T. and P.J.D. designed the experiments. K.LT performed experiments. K.L.T., K.W.G., and P.J.D. analyzed the data. K.L.T. and P.J.D. wrote the paper.

Abstract

Arousal state profoundly affects neural activity and vascular dynamics in the cortex, with sleep causing large changes in local field potentials (LFP) and increases in blood flow. Here we investigate how arousal state dictates the relationship between external measures of arousal, pupil diameter and blink rate, with neural activity and blood volume in the somatosensory cortex in both male and female head-fixed mice and determine whether optical measures of pupil diameter can accurately predict arousal state for classifying of neural data. Pupil diameter was consistently smaller during REM and NREM sleep than in the awake state. Pupil diameter changes were coherent with both changes in blood volume and gamma-band power in the somatosensory cortex, but the strength and sign of this relationship varied with behavioral state. We observed a strong negative correlation between pupil diameter and both blood volume and gamma-band power during periods of rest and sleep, though the correlations between pupil diameter and blood volume became positive during periods of alertness and active whisking, consistent with fidgeting and other body motions driving vasodilation in the somatosensory cortex. Blinking was associated with increases in arousal, and subsequent large decreases in blood volume when the mouse was asleep. Coherence of bilateral measures of gamma-band power and blood volume dropped immediately following a blink, indicating a 'reset' of vascular and neural activity. Using only pupil diameter, we could determine if the mouse is awake or asleep with high accuracy with a temporal resolution of seconds. Our results demonstrate a very strong reciprocal relationship between pupil diameter and hemodynamics signals in unanesthetized mice, reflecting the pronounced effects of arousal on cerebrovascular dynamics.

Introduction

The dynamics of the eyes can convey a great deal about the mental state of their owner. Besides their respective roles in controlling light levels and protecting the eye, both the diameter of the pupil and the rapid closing of the eyelid (blinking) can give signals about the state of neural activity in the brain (Strauch et al., 2022). Both of these measures are powerful, as they are non-invasive. However, for these measures to be useful, their relationship to neural and vascular physiology must be well-grounded. In addition to responding to levels of illumination, the diameter of the pupil reflects arousal level, with dilations associated with higher levels of arousal (Drew et al., 2001; Hess and Polt, 1964; Kahneman and Beatty, 1966; Morad et al., 2000; Onorati et al., 2013; Yoss et al., 1970). The pupil is an indicator of emotional arousal that correlates with increased sympathetic activity (Bradley et al., 2008) and will usually dilate when a subject is performing a task or making a decision (Burlingham et al., 2022; Einhauser et al., 2010; Gilzenrat et al., 2010; Hakerem and Sutton, 1966; Nassar et al., 2012). Recent rodent work has shown that pupil fluctuations track cortical state (McGinley et al., 2015; Reimer et al., 2014; Vinck et al., 2015). Pupil dilations reflect noradrenergic tone in the cortex and activity in the locus coeruleus in both rodents and primates (Joshi et al., 2016; Larsen and Waters, 2018; Preuschoff et al., 2011; Reimer et al., 2016). As head-fixed mice frequently sleep with their eyes open (Karimi Abadchi et al., 2020; Turner et al., 2020; Yuzgec et al., 2018), it has been observed that pupil diameter is lower during sleep and can be used detect sleep events minute-to-minute timescale (Karimi Abadchi *et al.*, 2020; Yuzgec *et al.*, 2018). Changes in pupil diameter are tightly coupled with BOLD fMRI signals seen neuromodulatory centers (Pais-Roldan et al., 2020; Sobczak et al., 2021). In addition to noradrenergic effects on neurons, noradrenergic input from the locus coeruleus causes vasoconstriction of cortical arteries (Bekar et al., 2012), coupling cortical hemodynamics to arousal.

In addition to its roles in protecting and lubricating the eye, blinking affected by mental state and fatigue (Holland and Tarlow, 1972; Nakamori et al., 1997; Stern et al., 1994; Van Orden et al., 2001). Humans blink every few seconds (Stern et al., 1984) though blinking is much less frequent in rats (Kaminer et al., 2011). Blink-rate is modulated by dopaminergic tone (Karson, 1983), often being elevated in those with schizophrenia (Karson, 1979; Karson et al., 1990). Blinking causes brief decreases in neural activity in visual areas (Gawne and Martin, 2000; Golan et al., 2016) that drive BOLD signals in the visual cortex (Bristow et al., 2005a; Bristow et al., 2005b; Hupe et al., 2012). Blinking also causes BOLD signals in both somatosensory regions (Guipponi et al., 2015) and the default mode network (Nakano et al., 2013), suggesting blinking is a brain-wide phenomena. However, the correlates of

blinking with arousal on a blink-by-blink basis are not as well understood.

To better understand how pupil diameter and blinking relate to neural activity and cortical hemodynamics across arousal states, we analyzed video of the eye with concurrent monitoring of neural activity and cortical blood volume in the somatosensory cortex of head-fixed mice of both sexes. We investigated the relationship between spontaneous changes in pupil diameter and these physiological signals in the awake state, as well as during REM and NREM sleep. We also tracked how neural activity and cortical blood volume changed around blinking events. Finally, using only changes in pupil diameter, we found that we can accurately detect spontaneous sleep events on a time scale of seconds providing a simple and robust measure of animal arousal for all studies employing head-fixed rodents.

Materials and Methods

Data here is from 22 C57BL/6J mice (12 males, Jackson Laboratory, Bar Harbor, ME) between the ages of 3 and 8 months of age. Data from 14 of these mice was previously published (Turner *et al.*, 2020) and we have added imaging/recordings from 8 more mice. We obtained a total of 442.75 hours of measurements (20.1 ± 5.3 hours per mouse) of naturally occurring awake (61.4 ± 17.3 %), NREM sleep (34.2 ± 16.1%), and REM sleep (4.4 ± 2.8%) data.

Animal procedures. This study was performed in accordance with the recommendations in the Guide for the Care and Use of Laboratory Animals of the National Institutes of Health. All procedures were performed in accordance with protocols approved by the Institutional Animal Care and Use Committee (IACUC) of Pennsylvania State University (protocol # 201042827). Surgical procedures are described in (Turner *et al.*, 2020; Winder et al., 2017). Briefly a head bar, cortical and muscle electrodes, and polished and reinforced thinned-skull windows (Drew et al., 2010; Shih et al., 2012) were surgically implanted under isoflurane anesthesia. Following surgery, animals were housed individually in a 12-hr. light/dark cycle with food and water ad libitum. Each animal was gradually acclimated to head-fixation in the week following recovery. Following the conclusion of imaging experiments, the animal was deeply anesthetized and transcardially perfused with heparin-saline followed by 4% paraformaldehyde for histological verification of electrode placement (Adams et al., 2018; Drew and Feldman, 2009).

Physiological data acquisition. Data were acquired with a custom LabVIEW program https://github.com/DrewLab/LabVIEW-DAQ (National Instruments, Austin, TX). For details on intrinsic optical signal imaging (IOS), electromyography (EMG), electrophysiology, whisker stimulation, and behavioral measurements see (Turner *et al.*, 2020; Zhang et al., 2022b). IOS reflectance was converted to changes in total hemoglobin (Δ[HbT]) using the Beer-Lambert law (Ma et al., 2016a; Ma et al., 2016b). Data was acquired in 15-minute intervals with a < 1 minute gap in between for saving data to disk.

Pupil diameter measurement. The pupil was illuminated with 780 nm light (measured at 0.02–0.05

mW/mm^2, Thorlabs S120VC) as mice are functionally blind to these wavelengths (Breuninger et al., 2011; Chang et al., 2013). To prevent constriction of the pupil by the illumination for IOS, a dichroic mirror located above the head was used to block as much of the IOS illumination from the eyes as possible, so that the mouse only saw a faint glow in its periphery (0.002–0.005 mW/mm^2) with no visible wavelength light shining directly into its eyes.

Data Availability. Processed data is available at [Dryad URL TBD]. Analysis code is available at [Temporarily GitHub URL - - https://github.com/KL-Turner/Turner-Manuscript2022]. Data was analyzed with code written by K.L.T, K.W.G, and P.J.D (MathWorks, MATLAB 2019b-2022a, Natick, MA).

Automated pupil diameter measurement and blink detection. Pupil diameter was extracted from videos made of the eye taken with a Basler GigE camera (acA640-120gm, Ahrensburg, Germany) with a 75 mm double Gauss, fixed focal length lens (#54-691, Edmond Optics Barrington, NJ) at 30 frames/second. Our pupil detection algorithm is adapted from the thresholding in Radon space algorithm developed to determine vessel cross-sections (Gao and Drew, 2014). The sclera and pupil were defined as the area within a user selected ROI created by outlining the first frame with the eye fully open. Images were inverted so that the pupil had the maximal intensity in the image. Images were 2-D median filtered ([5,5] x,y pixel median). The pixel intensity distribution was fit with a normal distribution using maximum likelihood estimation (MLE), and pixels above a threshold (average of 1 ± 0.25 standard deviations from the MLE) were set to 1 and all others to 0. The binarized image was then converted to Radon space and then normalized within each projection angle (Gao and Drew, 2014). A second threshold was applied prior to conversion back to image space and any holes within the filtered pupil object were filled. Frame-wise pupil area was calculated using a boundary classification algorithm. Occasional obstructions of the pupil (by a vibrissae) were identified by detecting rapid changes in pupil area. For these frames, the threshold used for thresholding in Radon space was iteratively decreased until the pixel area was within frame-wise change boundaries. MATLAB function(s): roipoly, medfilt2, imcomplement, mle, pdf, radon, iradon, bwboundaries, bwconvhull, imfill, regionprops, diff, fillmissing. Any periods where the pupil was obscured or otherwise unmeasurable were discarded from analysis.

Blink detection. Blinking was tracked independent of pupil diameter from the same ROI as used for pupil diameter measurements. Rapid changes in eye size were tracked using the sum of pixel intensities within the user defined ROI. For each frame all pixel intensities, sclera, and pupil, were summed and a frame-to-frame ROI intensity difference was calculated. As the eyelid obscures the eye during blinks, rapid changes in overall pixel intensity corresponded eyelid movements. A threshold was applied to binarize the frame wise differential and blinking events were extracted as above threshold frame-wise changes in image intensity. As subjects frequently blinked several times in rapid succession, blinking events that occurred with less than 1 second between successive blinks were concatenated in to blinking

bouts. Periods where a false-positive blink was detected, such as from the eye only partially closing, were also discarded. All detected blinking events were verified by manual inspection.

Electrophysiological analysis. Discrete LFP bands were digitally bandpass filtered from the broadband LFP data using a third-order Butterworth filter into the following bands: delta [1–4 Hz], theta [4–10 Hz], alpha [10–13 Hz], beta [13–30 Hz], gamma [30–100 Hz]. The filtered signal was then squared and low pass filtered < 10 Hz and resampled to 30 Hz. MATLAB function(s): butter, zp2sos, filtfilt, resample. Time frequency spectrograms were calculated using the Chronux toolbox, version 2.12 v03, function: mtspecgramc with a 5 second window and 1/5 second step size using [5,9] tapers and a passband of 1–100 Hz to encompass the local field potential (LFP). Electromyography (EMG, 300 Hz–3 kHz) from the nuchal (neck) muscles was bandpass filtered, squared, and convolved with a Gaussian kernel with a 0.5 second standard deviation, log transformed, and resampled down to 30 Hz. MATLAB function(s) butter, zp2sos, filtfilt, gausswin, log10, conv, resample.

Sleep scoring. Sleep states were scored consistent with previously published criteria (Cirelli, 2009; Saper and Fuller, 2017; Weber and Dan, 2016). NREM sleep is marked by predominantly elevated cortical delta-band [1–4 Hz] power and lower EMG tone during slow-wave (NREM sleep) (Amzica and Steriade, 1998; Steriade et al., 1993). Alternatively, REM sleep is seen with elevated hippocampal theta-band [4–10 Hz] power and elevated cortical gamma-band [30–100 Hz] power, and even further reduced EMG tone (muscle atonia) (Cantero et al., 2004; Le Van Quyen et al., 2010; Montgomery et al., 2008; Sullivan et al., 2014). Periods of awake rest greater than 5 seconds in duration with no whisker stimulation, no whisker motion, and no detectable body motion were identified. Pupil diameter z-scoring was done relative to these resting baseline periods. Sleep scoring was performed as in (Turner *et al.*, 2020). Every 5-second interval was classified as either Awake, NREM sleep, or REM sleep using a bootstrap aggregating random forest model with the predictors of cortical delta LFP, cortical beta LFP, cortical gamma LFP, hippocampal theta LFP, EMG power, heart rate, and whisking duration. Sleep model accuracy was validated using the out-of-bag error during model training. MATLAB function(s): TreeBagger, oobError, predict.

Pupil diameter during different arousal states. Pupil diameter (mm or z-units) was taken from *awake rest* events (≥ 10 sec induration), *awake whisking* (2–5 sec), *whisker stimulation*, *NREM sleep* (≥ 30 sec), and *REM sleep* (≥ 60 sec). Diameter was lowpass filtered (< 1 Hz) with a fourth-order Butterworth filter. MATLAB function(s): butter, zp2sos, filtfilt. Changes in whisking-evoked and stimulus-evoked (contralateral, auditory) diameters were taken as the change in diameter based on the 2 seconds prior to the onset of each event. Classification of *alert* or *asleep* were taken as 15-minute periods with no whisker stimulation and at least 80% of a given classification (Awake for *alert*, NREM/REM for *asleep*). The classification of *all* denotes all non-stimulation data independent of arousal state.

Power spectra and coherence. Spectral power was estimated using the Chronux function: mtspectrumc. For pre-whitening spectra, the first derivative was taken of the mean-subtracted data before the power calculation. Gamma-band power measurements were scaled by 1×10^{19} so that the order of magnitude changes (arbitrary units, a.u.) were more consistent with those of hemodynamic signal for direct comparison. MATLAB function(s): detrend, diff. Coherence analysis was run for each data type using the Chronux function: coherencyc. MATLAB function(s): detrend.

Cross-correlation. Data was low-pass filtered < 1 Hz using a fourth-order Butterworth filter and mean-subtracted. Cross-correlation analysis was run for each arousal state with either a ± 5 second or ± 30 second lag depending on duration. MATLAB function(s): xcorr, filtfilt, detrend.

Probability of sleep as a function of pupil diameter. The probability of being in each arousal state as a function of pupil diameter was obtained from the mean diameter during each 5 second sleep score and binning the value into a histogram, which was then smoothed with a median filter and Savitzky–Golay filter. MATLAB function(s): medfilt1, sgolayfilt.

Δ[HbT]/Gamma-band power vs. pupil relationship. Mean Δ[HbT] or gamma-band power (ΔP/P), and pupil diameter (z-units) during each arousal state classification was plotted as a 2D histogram to highlight clustering in each class (Awake, NREM, REM). MATLAB function(s): histogram2. Each classification was assigned a color and then the 3 images were merged as a composite in Fiji (ImageJ).

Pupil vs. Physiological model comparison. The pupil arousal scoring model was trained using either the z-unit diameter or mm diameter from training files that had accurate diameter detection. The physiological arousal scoring model was trained using the same data and parameters as those in the random forest arousal state classification model, but only using files with corresponding pupil diameters, so that the same files were used for training/testing for both model types. The model used for final comparison was a support vector machine classification algorithm, with 10-fold cross validation, receiver operator characteristic curves, and confusion matrices from each animal being calculated at the time of model training. MATLAB function(s): fitcsvm, crossval, kfoldloss, predict, fitposterior, resubPredict, perfcurve, confusionchart.

Experimental design and statistical analysis. Researchers were not blind to the experimental conditions or data analysis. Sample sizes are consistent with those of previously published studies (Echagarruga et al., 2020; Huo et al., 2015; Turner *et al.*, 2020; Winder *et al.*, 2017). Statistical evaluations were made using either generalized linear mixed-effects (GLME) models with the arousal state as a fixed effect, mouse identity as a random effect, and hemisphere (L/R, if applicable) as an interaction; or using a paired t-test for simpler comparisons. MATLAB function(s): fitglme, ttest2. Unless otherwise stated, statistical results report p-values from a GLME test. All reported quantifications are mean ± standard deviation unless otherwise indicated.

Results

Un-anesthetized mice were head-fixed under an intrinsic optical imaging setup (Huo et al., 2014; Sirotin and Das, 2009; Vazquez et al., 2014; Winder *et al.*, 2017) with concurrent electrophysiology to measure changes in neural activity from the vibrissa region of somatosensory cortex (Petersen, 2007; 2014). We concurrently tracked whisker motion (Winder *et al.*, 2017), electromyography of the nuchal muscles (Turner *et al.*, 2020), and pupil diameter/blinking (Larsen and Waters, 2018; Reimer *et al.*, 2014; Reimer *et al.*, 2016; Vinck *et al.*, 2015) **(Fig. 1a**). Using the thresholding in Radon space algorithm (Gao and Drew, 2014), we detected the pupil from video frames (**Fig. 1b-e, Video 1**). Blinks were detected from rapid pupil diameter changes (**Fig. 1f**). During the awake state, there are frequent bouts of whisker motion that are correlated with increases in pupil diameter, the EMG has high power, there is reduced low-frequency power in the LFP, and hemodynamic fluctuations are low except during periods of extended behavior or stimuli. During NREM sleep, whisker motion and EMG power are much lower than the awake state, and the pupil diameter is smaller. Cortical LFP and hemodynamic signals both begin to increase in amplitude with low frequency oscillations. During REM sleep, whisker motion increases along with eye movement, but the pupil remains highly constricted. Power in the EMG is at its lowest point due to muscle atonia (but with occasional twitches), and blood volume increases substantially above awake and NREM levels. A predominant theta-band is visible in the hippocampal LFP. An example of pupil diameter changes along with Δ[HbT] and the hippocampal LFP along with the arousal state is shown in **Fig. 1f.** This example shows that pupil diameter can be accurately tracked with concurrent neural, hemodynamic, and other behavioral measurements during periods of NREM and REM sleep.

Quantification of pupil diameter across arousal states

To quantify how fluctuations in pupil diameter change with arousal-state, we compared the pupil's diameter during several distinct arousal states and behaviors. Pupil diameter was highest during periods of active arousal and smallest during sleep. To standardize measures across animals and to account for slight differences in baseline illumination, we z-scored the pupil diameter to the mean and standard deviation during all periods of awake quiescence lasting at least 5 seconds in length. Italics denote arousal state criteria in subsequent discussion. All arousal state categories (*Rest*, *NREM*, *REM*, *Alert*, *Asleep*, *All*) excluded periods with whisker stimulation. *Rest*, defined as all periods of awake quiescence lasting at least 10 seconds in length, had a pupil diameter of 0.6 ± 0.17 mm **(Fig. 2a)** or -0.25 ± 0.88 z-units **(Fig. 2b)**. The mean z-unit during *Rest* was not zero because the minimum duration used for z-scoring (5

seconds) was shorter than that used for subsequent analysis (10 seconds). During volitional whisking bouts (lasting 2–5 seconds), pupil diameter increased to 0.89 ± 0.17 mm ($p < 2.3\times10^{-19}$ versus Rest) | 3.39 ± 0.88 z-units ($p < 2.1\times10^{-22}$). Brief stimulation of the vibrissae (10 psi of air for 0.1 seconds, directed so that it does not hit the face), pupil diameter increased 0.75 ± 0.18 mm ($p < 9.2\times10^{-8}$) | 1.95 ± 1.82 z-units ($p < 1.9\times10^{-11}$) for whisker stimulation. The pupil diameter decreased during *NREM* (> 30 seconds in length) to 0.35 ± 0.07 mm ($p < 8.1\times10^{-16}$) | -3.43 ± 0.64 z-units ($p < 6.2\times10^{-19}$) and even further as well during *REM* (> 60 seconds in length) to 0.26 ± 0.03 mm ($p < 3.2\times10^{-23}$) | -4.56 ± 0.75 z-units ($p < 2.3\times10^{-27}$). Periods of volitional whisking and whisker stimulation caused increases of 1.44 ± 0.47 z-units and 1.61 ± 0.62 z-units, respectively, in comparison to auditory controls which dilated the pupil by 0.98 ± 0.58 **(Fig. 2c)**. Note these increases are with respect to the z-unit diameter in the 2 seconds prior to event onset, which was a mixture of awake resting and volitional behaving data of various durations.

To look at changes in the power of the pupil diameter during different arousal states, we pre-whitened the diameter during periods of continuous *Rest* (> 10 seconds), continuous *NREM* (> 30 seconds), continuous *REM* (> 60 seconds), and 3 additional longer-length classifications (*Alert*, *Asleep*, and *All*) by taking the first derivative of the z-unit diameter prior to power estimation. *Alert* was classified as fifteen-minute periods classified with at least 80% of its model scores as 'Awake' whereas *Asleep* had 80% of the time in 'NREM' or 'REM' sleep, and *All* was all data. Two mice did not have any 15-minute periods that met the criteria for the *Alert* or *Asleep* categories (N = 20 mice) with the other four behaviors (*Rest, NREM, REM, All)* having N = 22 mice. Except for *REM*, once pre-whitened the power spectra of the pupil diameter during the longer length behaviors were similar to each other at the lower frequencies **(Fig. 2d)**. These findings support previous reports that the pupil increases with arousal and attention but decreases in size during periods of sleep.

Relationship between pupil diameter and hemodynamic and neural signals

We next asked how well the pupil diameter correlated with both neural and hemodynamic signals in the somatosensory cortex of mice both during awake behaviors and during different sleep stages. For each mouse, the pupil diameter was compared to both hemispheres' neural and hemodynamic signals, yielding 2*N measurements for each behavior, the non-independence (due to within animal correlations) was accounted for as an interaction in the statistical comparison (see Methods). To do this, we first looked at the coherence between hemodynamic signals, Δ[HbT], and the pupil diameter in z-units **(Fig. 2e)**. For nearly all cases, the coherence between pupil diameter and physiological signals was substantially higher at low frequencies. We evaluated the Δ[HbT]-pupil coherence during the different arousal states at a low frequency (0.02 Hz) and higher frequency (0.35 Hz) **(Fig 2f)**. These specific frequencies were chosen for statistical comparison (GLME) as they were the approximate peaks in Δ[HbT]-pupil coherence during

asleep behaviors and awake behaviors, respectively. At the low frequency of 0.02 Hz, coherence between total hemoglobin and pupil diameter during the *Alert* state was 0.32 ± 0.18 (N = 20 mice). Since we can only evaluate the 0.02 Hz component of the spectrum in the longer 15-minute duration behavioral epochs, statistical comparisons for longer durations conditions were done relative to *Alert*, which consisted of a mixture of awake rest, volitional whisking, and other fidgeting behaviors. Δ[HbT]-pupil coherence during *Asleep* behavior (which comprised of mostly 'NREM'/'REM' periods), was 0.79 ± 0.06 ($p < 2.0\times10^{-29}$) and *All* periods was 0.58 ± 0.17 ($p < 9.3\times10^{-14}$). At 0.35 Hz, statistical comparisons were done relative to *Rest*, which had a Δ[HbT]-pupil coherence of 0.51 ± 0.06. The Δ[HbT]-pupil coherence during rest was non statistically different than that during the *Alert* behavior, being 0.52 ± 0.09 (n.s, $p < 0.33$). However, the coherence at 0.35 Hz was significantly lower during all sleep associated periods – *NREM*: 0.3 ± 0.11 ($p < 7.0\times10^{-33}$); *REM*: 0.15 ± 0.08 ($p < 9.8\times10^{-66}$); *Asleep*: 0.29 ± 0.12 ($p < 2.3\times10^{-33}$), *All* data was 0.42 ± 0.1 ($p < 3.7\times10^{-8}$). These show that low-frequency fluctuations in blood volume are highly correlated to the pupil diameter, suggesting that the same processes that modulate arousal on these timescales also cause constriction in the cerebral vasculature.

We then looked at the cross-correlation between Δ[HbT] and pupil diameter to determine their temporal relationship. We saw the peak correlation during awake *Rest* was -0.37 ± 0.25 at a lag of 1.13 seconds, i.e., pupil diameter changes occurred on average 1.13 seconds before hemodynamic oscillations and were anti-correlated **(Fig. 2g)**. *NREM* was more strongly anti-correlated than *Rest* at -0.56 ± 0.08 at a lag of 0.73 seconds. *REM* had a positive correlation of 0.24 ± 0.11 at a lag of 1.97 seconds. The peak of the Δ[HbT] and pupil diameter correlation in the *Alert* condition was 0.1 ± 0.21 at a lag of -0.43 seconds, this negative lag is likely due to sustained bouts of whisking **(Fig. 2h)**. *Asleep* and *All* were anti-correlated at -0.65 ± 0.08 at a lag time of 1.0 seconds and -0.48 ± 0.15 at a lag of 1.23 seconds respectively. Generally, pupil dilations preceded vasoconstriction by a second or so.

We repeated the same coherence and cross-correlation analysis for the envelope of gamma-band power (ΔP/P) and pupil diameter in z-units, which showed a similar trend for most arousal states to those seen in Δ[HbT]-pupil comparisons. The gamma-pupil coherence during long *Alert* periods at 0.02 Hz was 0.34 ± 0.18 **(Fig. 2i, j)**, being significantly elevated during periods of asleep at 0.68 ± 0.09 ($p < 2.4\times10^{-18}$) and during *All* data at 0.48 ± 0.19 ($p < 2.9\times10^{-5}$). Gamma-pupil coherence at 0.35 Hz during periods of awake *Rest* and *Alert* was similar, at 0.2 ± 0.1 and 0.2 ± 0.09 (n.s, $p < 0.58$), similar to what is seen between the pupil diameter and cortical neuron membrane potential (McGinley *et al.*, 2015). All other arousal states were significantly lower than those of the primary awake states; *NREM*: 0.09 ± 0.06 ($p < 2.9\times10^{-13}$); *REM*: 0.14 ± 0.08 ($p < 3.7\times10^{-5}$); *Asleep*: 0.11 ± 0.07 ($p < 9.8\times10^{-9}$); *All*: 0.11 ± 0.08 ($p < 5.3\times10^{-9}$) **(Fig. 2i, j)**. The peak cross-correlation during *Rest* was -0.16 ± 0.20 at a lag time of -0.07 seconds **(Fig. 2k)** and during *Alert* was -0.02 ± 0.14 at a lag time of 0.1 seconds **(Fig. 2l)**, indicating very

little time difference between cortical gamma-band and pupil diameter fluctuations during awake behaviors. Peaks during sleeping periods occurred at *NREM*: -0.26 ± 0.06 at a lag time of -0.1 seconds; *REM*: 0.05 ± 0.04 at a lag time of 1.53 seconds; *Asleep*: -0.32 ± 0.05 at a lag time of -0.43 seconds; and *All*: -0.23 ± 0.11at a lag time of -0.2 seconds. There was a strong negative correlation between pupil diameter and blood volume as well as between pupil diameter and gamma-band power during periods of rest and sleep, with these correlations turning positive during periods of alertness and active whisking. This is in general consistent with an anticorrelation between arousal level and blood volume in the absence of stimulation or active whisking behavior.

Blinking is associated with increases in arousal

We next wanted to explore the relationship between blinking and arousal level. We quantified inter-blink intervals (Fig 3a.). Our mice had a mean inter-blink interval of 117.4 seconds ± 33.6 seconds (**Fig. 3b**, N = 22 mice). We then quantified the probability of a blink being triggered by a whisker stimulus. Except for one animal, our mice did not frequently blink after a whisker stimulus, with the mean probability of blinking within 5 seconds post-stimulus being only 5.4 ± 5.1% (**Fig. 3c**, N = 21 mice, excluded mouse 25.6%). For blinks that did occur post-stimulus, blinks typically occurred within the first half-second (~37%) and the probability decreased thereafter. Blinks primarily occurred during the awake state (> 70%), but when they did occur during periods of NREM or REM sleep the animal either quickly returned to sleep upon brief waking or did not wake up at all **(Fig. 3d)**. Our mice frequently slept with their eyes completely open (Turner *et al.*, 2020; Yuzgec *et al.*, 2018), and even had blinking events occur during prolonged periods of maintained REM sleep. The likelihood of volitional whisking occurring simultaneously with blinking behavior was high **(Fig. 2e)** occurring nearly 40% of the time with blinks that occurred during awake periods, and lesser so during periods where the blink occurred either during or immediately following periods that were asleep (combination of NREM and REM classification scores, with the majority being NREM).

As blinks commonly occurred in clusters, for all blink-related analysis, we only looked at the first blink occurring in a string of blink events that occur within less than 1 second of each other. All blinks that occurred within ± 5 seconds of whisker stimulation were also excluded to prevent the stimulus from interfering with the blink-triggered comparison. To help separate the effect of the blink from the effect of volitional whisking behavior coinciding with it, we split the data set into low whisk blinks (LWB) and high whisk blinks (HWB) for both the awake and asleep arousal states. Low-whisk blinks were defined as events where the mouse was whisking for less than 1/3 of a second in the 2 seconds surrounding each blink, whereas high-whisk blinks were defined as whisking for greater than 1 second within ±2 seconds of the blink. We evaluated blink-triggered averages for changes in diameter (z-units), total hemoglobin

(Δ[HbT]), EMG power, cortical LFP, and hippocampal LFP across all blinks from all mice that met the desired criteria. During the awake state, low whisks blinks caused an increase of around 0.7 z-units in pupil diameter compared to resting baseline, while high whisk blinks caused an increase in excess of 3 z-units **(Fig. 3f)**. Note the small drop in diameter occurring immediately after the blink, which corresponds to the eye being partially obscured as the eyelids close. The pupil tracking algorithm interpolates missing frames when the eye is (briefly) closed during a blink but will still approximate the pupil when the eye is partially closing/opening resulting in the small dip. Δ[HbT] during low whisk blinks increased around 4 µM from the time prior to the blink, whereas high-whisk blinks increased around 10 µM due to the increased whisking in the time preceding the blink **(Fig. 3g)**. EMG power increases ~0.6 orders of magnitude during low-whisk blinks compared to 1.2 orders of magnitude during high-whisk blinks, with power increases starting about 0.5 seconds before the blink occurs. There were negligible increases in gamma-band power in both the somatosensory cortex **(Fig. 3i)** and the CA1 hippocampus **(Fig. 3k)** during low whisk blinks, with the ~20% increases in power seen during high whisking largely being attributed to the whisking (Winder *et al.*, 2017) and not the blink **(Fig. 3j, l)**.

Blink-associated changes were similar during blinks that occurred during periods of sleep, with key differences in the baseline determined by arousal state. Pupil diameter during both high and low whisk asleep blinks was greatly reduced (< -3 z-units) prior to the blink, with the diameter slowly increasing preceding the blink as the animal began to wake up. For periods of low whisking, the diameter remained constricted as the animals presumable fell back asleep or remained asleep **(Fig. 3m)**. Changes in hemodynamics follow a similar trend, with there being a reduction in total hemoglobin in the time preceding the blink as the animals are waking up **(Fig. 3n)**. EMG power changes were similar to the awake blink, but with a lower baseline power **(Fig. 3o)**. We noted no significant differences in blink-associated power spectra during blinks that occurred around sleeping periods **(Fig. 3p, q, r, s)**, however the drop in cortical delta power around blink is evident as the animals wake up from NREM sleep. Altogether, blinking was associated with increases in arousal, but to varying degrees marked by differing amounts of accompanying whisking. When blinks occurred during the awake state, there was only a small increase in blood volume when there was minimal whisking. However, when blinks occurred during periods of sleep, large decreases in blood volume followed regardless of whisking amount.

Awake blinking causes a resetting of neural and vasculature activity

We next asked how blinking affected the synchronicity between bilateral regions of somatosensory cortex. Anecdotally, processing of new or startling information is accompanied by blinking, suggesting it is associated with some sort of mental 'resetting'. As before, we separated blinks by arousal state (awake, asleep) and looked at the changes in power and coherence during periods preceding (-15 seconds to -5

seconds) and following (5 seconds to 15 seconds) each blink. We excluded the time ± 5 seconds adjacent to each blink to capture the pre/post effects of the blink on synchronicity and not the blink itself. For both bilateral cortical gamma-band power signals and bilateral changes in total hemoglobin, we evaluated the power/coherence changes from 0 to 0.2 Hz as this corresponded to the period of the largest difference between pre and post blink. One animal was excluded from Figure 4's analysis due to being an outlier in its blink rate (N = 21) and statistics were evaluated using a paired t-test. Coherence between bilateral gamma-band power signals during the awake state dropped following a blink from [pre-blink] 0.38 ± 0.13 to [post-blink] 0.28 ± 0.10 ($p < 0.0104$) **(Fig. 4a, b)**. Power in these signals was highly variable **(Fig 4c)** and did not change in the period following a blink, [pre-blink] 13.2 ± 81.0 a.u. vs. [post-blink] 11.9 ± 73.7 a.u. ($p < 0.938$**) (Fig. 4d)**. There was no clear relationship between changes in gamma-band power pre/post blink vs. changes in bilateral gamma-band coherence pre/post blink **(Fig. 4e)**. Awake bilateral Δ[HbT] coherence was [pre-blink] 0.88 ± 0.03 dropping to [post-blink] 0.84 ± 0.05 ($p < 0.0024$) **(Fig. 4f, g)**. Unlike the gamma-band power, there was a significant drop in cortical hemodynamic power following a blink: [pre-blink] 149.1 ± 49.1 a.u. vs. [post-blink] 100.4 ± 33.3 a.u. ($p < 8.8\times10^{-7}$) **(Fig. 4h, i)**, and these appear to be related **(Fig. 4j)**.

For blinks that occurred during sleep, neither the gamma-band power nor total hemoglobin showed any significant changes between pre- and post-blink power or coherence. Coherence between bilateral gamma-band signals during asleep blinks was [pre-blink] 0.44 ± 0.18 vs. [post-blink] 0.46 ± 0.17($p < 0.702$) **(Fig. 4k, l)** with power changes of [pre-blink] 7.0 ± 34.4 vs. [post-blink] 7.1 ± 39.9 ($p < 0.995$) **(Fig. 4m, n)** with no relationship between power and coherence changes **(Fig. 4o)**. Bilateral hemodynamic coherence was [pre-blink] 0.89 ± 0.04 vs. [post-blink] 0.89 ± 0.04 ($p < 0.678$) **(Fig. 4p, q)** at a power of [pre-blink] 187.1 ± 67.1 vs. [post-blink] 174.1 ± 47.3 ($p < 0.308$) **(Fig. 4r, s)** with no relationship between power and coherence changes **(Fig. 4t)**. This indicates that blinking during the awake state leads to a 'resetting' of neural and vascular signals, but with no such changes seen during sleep.

Pupil diameter strongly predicts arousal-state

Finally, we wanted to explore the pupil's use as a predictor of arousal state by comparing its predictive power to that of more conventional sleep scoring physiological parameters (cortical delta power, hippocampal theta power, EMG). As pupil diameter is commonly measured in behaving mouse paradigms (Musall et al., 2019; Stringer et al., 2019; Vinck *et al.*, 2015), arousal scoring using pupil diameter could be very useful for detecting bouts of sleep when other more invasive assays are not available. Previous work has shown that the sleep/wake state of head-fixed mice can be determined accurately on the timescale of hundreds of seconds (Yuzgec *et al.*, 2018), but here we asked if it can be

done on a time scale of seconds, which would allow the detection of short sleep bouts that could confound behavioral experiments.

To get an idea of how pupil diameter differs across arousal states, we plotted the probability of being in each arousal state as a function of pupil diameter in z-units **(Fig. 5a)**. It was clear that the pupil diameter could be used to differentiate the 'Awake' arousal state from the NREM and REM states (with a threshold of around -2 z-units). However, there much less separation of pupil diameter between sleep states. Therefore, we simplified our model classification to 'Asleep', which is a combination of 'NREM' and 'REM' states. While the pupil highly correlates to both gamma-band power **(Fig. 5b)** and hemodynamic changes **(Fig. 5c),** with clear separation between arousal states, the pupil's diameter during 'NREM' was very close to its diameter 'REM'. We compared the manual scores of an entire day's imaging session to those produced by two new classification models, one using seven physiological parameters (i.e., 'Physiological model', see Materials and Methods) and the other using only the pupil (z-units) as a single predictor (i.e., 'Pupil model'). When 'NREM' and 'REM' periods are simplified as 'Asleep', the Pupil model captures the pupil diameter during prolonged periods of sleep, even better than physiological model at capturing periods of REM sleep **(Fig. 5d)**. For each model we manually scored two of the six days of data, or ~1/3 of the total data set with 5 second temporal resolution. Alternating 15-minute-long files were then split into two groups, one for model training and one for model validation. The example from Figure 5d was a manually scored day that was not used in that animal's model training or validation. The pupil model's decision boundary for the representative example was -2.27 z-units. A scatter plot with sleep/wake boundaries for each mouse is shown in **Fig. 5e**. The average boundary in z-units from each animal's model was -1.75 ± 0.8 z-units (N = 22 mice). When running each model using diameter in mm instead of z-units, the average decision boundary was 0.46 ± 0.1 mm **(Fig. 5f)**. With respective to identifying sleep, the Physiological model had a sensitivity (recall) of 90.5%, specificity (selectivity) of 94%, precision of 92.1%, and negative predictive value of 92.7%. This corresponded to a total accuracy of 92.5% **(Fig. 5g)**. The Pupil model had a sensitivity of 85.3%, specificity of 91.3%, precision of 88.3%, negative predictive value of 89.0%, and total accuracy of 88.7% **(Fig. 5h)**. During model training, we evaluated the model from each animal using 10-fold cross-validation. The average loss from physiological models was 0.07 ± 0.02 and from pupil models was 0.11 ± 0.03 ($p < 1.6\times10^{-7}$) **(Fig. 5i)**. We then compared the coherence between each model's predictions and the manual classifications, which demonstrates how well each model captures continuous events (either awake or asleep) of different durations **(Fig. 5j)**. Both models perform better at predicting longer, continuous length events than they do at predicting short duration events. This translates to each model being better at predicting 1-minute of a constant classification than it is during periods where the arousal-state is fluctuating (such as drowsy periods and transitions). The Physiological model had a greater coherence with the manually scored

classifications than the Pupil model at all frequencies. Still, the Pupil model performed markedly well as an awake-asleep classifier with an average area under the curve (receiver operator characteristic) of 0.94 ± 0.02 **(Fig. 5k)**. These result show that pupil diameter can be a non-invasive approach to determine if head fixed mice are sleeping on a timescale of seconds.

Discussion

In this study, we explored the relationships between pupil diameter and blink rate with ongoing neural activity and hemodynamic signals in the somatosensory cortex of mice in different arousal states. Because our mice frequently slept, when averaged over the entire data set, the pupil diameter was strongly anti-correlated with blood volume and gamma-band power due to the large vasodilation occurring during sleep (Turner *et al.*, 2020). When restricted to just to data in the awake state (whose neural and hemodynamic signals are dominated by body movements and fidgeting behavior (Drew et al., 2020; Drew et al., 2019; Musall *et al.*, 2019; Salkoff et al., 2020; Stringer *et al.*, 2019; Winder *et al.*, 2017)), the pupil diameter was positively correlated with blood volume and gamma-band power. The coherence between pupil diameter and blood volume was stronger at lower frequencies and was highest (>0.75) at 0.02 Hz (corresponding to a ~50 second period) in the sleeping mouse. Interestingly, activity in the locus coeruleus (LC) and the concentration of norepinephrine (which is vasoconstrictory) during NREM sleep fluctuates on a similar timescale (Osorio-Forero et al., 2021). These observations are consistent with noradrenergic tone being vasoconstrictory (Bekar *et al.*, 2012; Goadsby et al., 1985; Raichle et al., 1975), but also being highest during periods of body motion and arousal, when local vasodilatory signals from neurons are highest (Echagarruga *et al.*, 2020; Winder *et al.*, 2017; Zhang et al., 2019).

Blinking was associated with changes in arousal levels and in the neural and vascular physiology. Mice were more likely to be in awake state after blinking than before, and bilateral synchronization in the gamma-band envelope decreased after blinks in the awake state. Pupil diameter was consistently smaller during sleep states and larger during the awake state, allowing the pupil to be used as a predictor of arousal state (Yuzgec *et al.*, 2018). As a practical matter, our results show that monitoring the pupil can provide a second-by-second insight into the sleep wake state of mice. Since pupil monitoring is non-invasive and can be performed to detect periods of sleep which are common well-acclimated, head-fixed mice. These periods of sleep can be an issue not only in behavioral tasks, but also in studies looking at spontaneous activity. In human studies, sleep episodes contaminate resting state studies (Tagliazucchi and Laufs, 2014). In mice, neural and hemodynamic correlations are much higher during sleep (Turner *et al.*, 2020). Detecting and monitoring arousal changes is essential for correct interpretation of any resting-state study (Drew *et al.*, 2020; Liu et al., 2018; Tagliazucchi and Laufs, 2014).

Our findings that the pupil diameter was strongly anticorrelated with blood volume should be taken the context of the literature relating arousal and pupil diameter to locus coeruleus activity, and the vasoconstrictory impact of the noradrenergic (NE) inputs of LC activity the cerebral vasculature. The NE levels in the brain track LC neuron activity (Berridge and Abercrombie, 1999; Feng et al., 2019). Sensory stimuli drive increases in LC neural activity, NE tone, and pupil dilation (Gilzenrat *et al.*, 2010; Gray et al., 2021; Joshi *et al.*, 2016; Murphy et al., 2014; Schwarz and Luo, 2015; Yang et al., 2021) (though the correlations between pupil diameter and spiking of individual LC neurons is low (Megemont et al., 2022)). Activation of noradrenergic neurons in the LC drive awakening from sleep (Carter et al., 2010; Hayat et al., 2020; Kjaerby et al., 2020), and awakening from sleep is followed by profound vasoconstriction (Turner *et al.*, 2020) and brain-wide hemodynamic changes (Fultz et al., 2019; Liu *et al.*, 2018; Liu et al., 2015; Zhang et al., 2022a). Electrical stimulation of the LC and increases in NE levels (Bekar *et al.*, 2012) cause vasoconstriction (Goadsby *et al.*, 1985; Raichle *et al.*, 1975) (but see (Toussay et al., 2013)). However, we saw that the pupil diameter-blood volume correlation was positive in the *Alert* state, which seems to contradict the vasoconstrictory nature of NE. The *Alert* state contains many fidgeting and whisking bouts, which are body movements. While NE is known to rise during locomotion (Paukert et al., 2014; Polack et al., 2013) and movement (Feng *et al.*, 2019), the activity of vasodilatory nNOS neurons (Echagarruga *et al.*, 2020) and vasodilatory extracellular potassium levels are both elevated by locomotion (Longden et al., 2017; Rasmussen et al., 2019), and these two vasodilators are likely strong enough to drive vasodilation even the face of elevated NE. Furthermore, the magnitude of NE increases during movement are much smaller that the decreases during sleep. During sleep, cortical NE levels fall >50% (Bellesi et al., 2016; Kjaerby *et al.*, 2020), but arousal-induced increase above the baseline during voluntary body movements and fidgeting are of a substantially smaller magnitude (Feng *et al.*, 2019), which would explain why vasodilation dominates in these behaviors. The strong correlation of pupil diameter to blood volume is consistent with noradrenergic modulation being a strong contributor to neurovascular coupling.

Figure Legends

Fig. 1 | Pupil diameter is highly dependent on arousal-state

(a) Photograph and schematic of the experimental setup. IOS imaging of the whisker portion of somatosensory cortex collected using an illumination wavelength at an isosbestic point of hemoglobin (530 nm or 568 nm) through bilateral thinned-skull windows. Electrodes were implanted into somatosensory cortex layer 5 and into hippocampal CA1. EMG electrodes were also implanted into the nuchal muscles of the neck. A camera directed towards the whisker pad captures motion for behavioral

characterization. An additional camera directed toward the eye, illuminated by infrared 780 nm light, captures changes in pupil diameter and blinking. Directed air puffers allow controlled stimulation of the left/right whisker pad, as well as auditory controls. **(b)** Pupil is detected by drawing an ROI around the mouse's eye. **(c)** Maximum-likelihood-estimate of pixels within the ROI show separation between the pupil and sclera in the inverted image. A threshold is then set for initial diameter estimation. **(d)** Image of pupil that has been thresholded in Radon space after it is transformed back into image space. **(e)** Detected pupil superimposed on video frame. **(f)** Example showing changes in pupil diameter, whisker motion, EMG power, Δ[HbT], and CA1 LFP during awake, NREM, and REM periods.

Fig. 2 | Pupil diameter is highly correlated with blood volume and gamma-band power during different arousal states

(a) Mean pupil diameter (mm) during each arousal state. Mean of each animal is a circle. Grey diamond and error bars are mean ± std. across animals for each arousal state. **(b)** Mean pupil diameter (z-units) during each arousal state. **(c)** Whisking-evoked and stimulus evoked increases in pupil diameter based on the 2 seconds prior to event onset. **(d)** Pre-whitened power spectrum of pupil diameter (z-units) during different arousal states. **(e-h)** Comparison of Δ[HbT] vs. pupil diameter **(e)** Coherence. **(f)** Coherence at 0.02 and 0.35 Hz. **(g)** Cross-correlation for short duration events **(h)** Cross-correlation for long duration events. **(i-l)** Comparison of gamma-band power vs. pupil diameter **(i)** Coherence. **(j)** Coherence at 0.02 and 0.35 Hz. **(k)** Cross-correlation for short duration behaviors. **(l)** Cross-correlation for long-duration behavioral classifications. Line graph error bars **(c, d, g, h, k, l)** are standard error of the mean. GLME *$p < 0.05$, **$p < 0.01$, ***$p < 0.001$, n.s. – not significant.

Fig. 3 | Blink-triggered neural and blood volume responses show arousal state-dependent changes

(a) Histogram of inter-blink interval for all blinks. **(b)** Mean inter-blink interval from each animal. **(c)** (main plot) Location probability of a blink if occurring after whisker stimulation (inset scatter) Mean probability from each animal of blinking after a whisker stimulus. **(d)** Arousal state classification probability surrounding blinking periods. **(e)** Probability of whisking prior to a blink if the blink occurs during awake or asleep periods. **(f-l)** Blink-triggered averages for blinks that occurred during an awake period, separated into either high whisking or low whisking events. **(f)** Diameter during awake blinks **(g)** Hemodynamics during awake blinks **(h)** Electromyography during awake blinks. **(i)** Cortical LFP during awake blinks with low amounts of whisking. **(j)** Cortical LFP during awake blinks with high amounts of whisking. **(k)** Hippocampal LFP during awake blinks with low amounts of whisking. **(l)** Hippocampal LFP during awake blinks with high amounts of whisking. **(m-s)** Blink-triggered averages for blinks that

occurred during an asleep period, separated into either high whisking or low whisking events. **(m)** Diameter during asleep blinks **(n)** Hemodynamics during asleep blinks **(o)** Electromyography during asleep blinks. **(p)** Cortical LFP during asleep blinks with low amounts of whisking. **(q)** Cortical LFP during asleep blinks with high amounts of whisking. **(r)** Hippocampal LFP during asleep blinks with low amounts of whisking. **(s)** Hippocampal LFP during asleep blinks with high amounts of whisking. Scatter plot error bars **(b, c inset)** are standard deviation. Line graph error bars **(c main, e, f, g, h, m, n, o)** are standard error of the mean.

Fig. 4 |Effects of blinking on neural and bilateral hemodynamic signals

(a-e) Gamma-band leading and lagging an awake blink **(a)** Coherence between bilateral gamma-band signals **(b)** Coherence evaluated from 0 to 0.2 Hz **(c)** Gamma-band power **(d)** Power evaluated from 0 to 0.2 Hz **(e)** Change in pre/post blink power vs. change in pre/post blink coherence **(f-j)** Δ[HbT] leading and lagging an awake blink **(f)** Coherence between bilateral hemodynamic signals **(g)** Coherence evaluated from 0 to 0.2 Hz **(h)** Δ[HbT] power **(i)** Power evaluated from 0 to 0.2 Hz **(j)** Change in pre/post blink power vs. change in pre/post blink coherence. **(k-o)** Gamma-band leading and lagging an asleep blink **(k)** Coherence between bilateral gamma-band signals **(l)** Coherence evaluated from 0 to 0.2 Hz **(m)** Gamma-band power **(n)** Power evaluated from 0 to 0.2 Hz **(o)** Change in pre/post blink power vs. change in pre/post blink coherence. **(p-t)** Δ[HbT] leading and lagging an asleep blink **(p)** Coherence between bilateral hemodynamic signals **(q)** Coherence evaluated from 0 to 0.2 Hz **(r)** Δ[HbT] power **(s)** Power evaluated from 0 to 0.2 Hz **(t)** Change in pre/post blink power vs. change in pre/post blink coherence. Scatter plot error bars **(b, d, g, i, l, n, q, s)** are standard deviation. Line graph error bars **(a, c, f, h, k, m, p, r)** are standard error of the mean. Paired t-test *$p < 0.05$, **$p < 0.01$, ***$p < 0.001$, n.s. – not significant.

Fig. 5 |Pupil diameter alone is an effective predictor of arousal state

(a) Probability of arousal state classification as a function of pupil diameter **(b)** Relationship between pupil diameter and gamma-band power during each arousal state **(c)** Two-dimensional histogram showing the relationship between pupil diameter and Δ[HbT] during each arousal state **(d)** Hypnogram comparison of manual, physiological model, and pupil model arousal state scores for the entire imaging session from the representative animal in Figure 1. **(e)** Visualization of the pupil model (SVM) hyperplane decision boundary **(f)** Decision boundary (diameter, mm) from each animal using pupil model **(g)** Physiological model confusion matrix **(h)** Pupil model confusion matrix **(i)** 10-fold cross validation comparison between the two models **(j)** Coherence between manual scoring of sleep/wake state and scoring of the physiological and pupil models. **(k)** Receiver operator characteristic curves for the pupil model and

subsequent area under the curve (AUC) from each animal. Scatter plot error bars **(f, i, k inset)** are standard deviation. Line graph error bars **(j)** are standard error of the mean. Paired t-test *$p < 0.05$, **$p < 0.01$, ***$p < 0.001$, n.s. – not significant.

References

Adams, M.D., Winder, A.T., Blinder, P., and Drew, P.J. (2018). The pial vasculature of the mouse develops according to a sensory-independent program. Sci Rep *8*, 9860. 10.1038/s41598-018-27910-3.

Amzica, F., and Steriade, M. (1998). Electrophysiological correlates of sleep delta waves. Electroencephalogr Clin Neurophysiol *107*, 69-83. 10.1016/s0013-4694(98)00051-0.

Bekar, L.K., Wei, H.S., and Nedergaard, M. (2012). The locus coeruleus-norepinephrine network optimizes coupling of cerebral blood volume with oxygen demand. J Cereb Blood Flow Metab *32*, 2135-2145. 10.1038/jcbfm.2012.115.

Bellesi, M., Tononi, G., Cirelli, C., and Serra, P.A. (2016). Region-Specific Dissociation between Cortical Noradrenaline Levels and the Sleep/Wake Cycle. Sleep *39*, 143-154. 10.5665/sleep.5336.

Berridge, C.W., and Abercrombie, E.D. (1999). Relationship between locus coeruleus discharge rates and rates of norepinephrine release within neocortex as assessed by in vivo microdialysis. Neuroscience *93*, 1263-1270. Doi 10.1016/S0306-4522(99)00276-6.

Bradley, M.M., Miccoli, L., Escrig, M.A., and Lang, P.J. (2008). The pupil as a measure of emotional arousal and autonomic activation. Psychophysiology *45*, 602-607. 10.1111/j.1469-8986.2008.00654.x.

Breuninger, T., Puller, C., Haverkamp, S., and Euler, T. (2011). Chromatic bipolar cell pathways in the mouse retina. J Neurosci *31*, 6504-6517. 10.1523/JNEUROSCI.0616-11.2011.

Bristow, D., Frith, C., and Rees, G. (2005a). Two distinct neural effects of blinking on human visual processing. Neuroimage *27*, 136-145. 10.1016/j.neuroimage.2005.03.037.

Bristow, D., Haynes, J.D., Sylvester, R., Frith, C.D., and Rees, G. (2005b). Blinking suppresses the neural response to unchanging retinal stimulation. Curr Biol *15*, 1296-1300. 10.1016/j.cub.2005.06.025.

Burlingham, C.S., Mirbagheri, S., and Heeger, D.J. (2022). A unified model of the task-evoked pupil response. Sci Adv *8*, eabi9979. 10.1126/sciadv.abi9979.

Cantero, J.L., Atienza, M., Madsen, J.R., and Stickgold, R. (2004). Gamma EEG dynamics in neocortex and hippocampus during human wakefulness and sleep. Neuroimage *22*, 1271-1280. 10.1016/j.neuroimage.2004.03.014.

Carter, M.E., Yizhar, O., Chikahisa, S., Nguyen, H., Adamantidis, A., Nishino, S., Deisseroth, K., and de Lecea, L. (2010). Tuning arousal with optogenetic modulation of locus coeruleus neurons. Nat Neurosci *13*, 1526-1533. 10.1038/nn.2682.

Chang, L., Breuninger, T., and Euler, T. (2013). Chromatic coding from cone-type unselective circuits in the mouse retina. Neuron *77*, 559-571. 10.1016/j.neuron.2012.12.012.

Cirelli, C. (2009). The genetic and molecular regulation of sleep: from fruit flies to humans. Nat Rev Neurosci *10*, 549-560. 10.1038/nrn2683.

Drew, P., Sayres, R., Watanabe, K., and Shimojo, S. (2001). Pupillary response to chromatic flicker. Exp Brain Res *136*, 256-262. 10.1007/s002210000605.

Drew, P.J., and Feldman, D.E. (2009). Intrinsic signal imaging of deprivation-induced contraction of whisker representations in rat somatosensory cortex. Cereb Cortex *19*, 331-348. 10.1093/cercor/bhn085.

Drew, P.J., Mateo, C., Turner, K.L., Yu, X., and Kleinfeld, D. (2020). Ultra-slow Oscillations in fMRI and Resting-State Connectivity: Neuronal and Vascular Contributions and Technical Confounds. Neuron *107*, 782-804. 10.1016/j.neuron.2020.07.020.

Drew, P.J., Shih, A.Y., Driscoll, J.D., Knutsen, P.M., Blinder, P., Davalos, D., Akassoglou, K., Tsai, P.S., and Kleinfeld, D. (2010). Chronic optical access through a polished and reinforced thinned skull. Nat Methods *7*, 981-984. 10.1038/nmeth.1530.

Drew, P.J., Winder, A.T., and Zhang, Q. (2019). Twitches, Blinks, and Fidgets: Important Generators of Ongoing Neural Activity. Neuroscientist *25*, 298-313. 10.1177/1073858418805427.

Echagarruga, C.T., Gheres, K.W., Norwood, J.N., and Drew, P.J. (2020). nNOS-expressing interneurons control basal and behaviorally evoked arterial dilation in somatosensory cortex of mice. Elife *9*. 10.7554/eLife.60533.

Einhauser, W., Koch, C., and Carter, O.L. (2010). Pupil dilation betrays the timing of decisions. Front Hum Neurosci *4*, 18. 10.3389/fnhum.2010.00018.

Feng, J., Zhang, C., Lischinsky, J.E., Jing, M., Zhou, J., Wang, H., Zhang, Y., Dong, A., Wu, Z., Wu, H., et al. (2019). A Genetically Encoded Fluorescent Sensor for Rapid and Specific In Vivo Detection of Norepinephrine. Neuron *102*, 745-761 e748. 10.1016/j.neuron.2019.02.037.

Fultz, N.E., Bonmassar, G., Setsompop, K., Stickgold, R.A., Rosen, B.R., Polimeni, J.R., and Lewis, L.D. (2019). Coupled electrophysiological, hemodynamic, and cerebrospinal fluid oscillations in human sleep. Science *366*, 628-631. 10.1126/science.aax5440.

Gao, Y.R., and Drew, P.J. (2014). Determination of vessel cross-sectional area by thresholding in Radon space. J Cereb Blood Flow Metab *34*, 1180-1187. 10.1038/jcbfm.2014.67.

Gawne, T.J., and Martin, J.M. (2000). Activity of primate V1 cortical neurons during blinks. J Neurophysiol *84*, 2691-2694. 10.1152/jn.2000.84.5.2691.

Gilzenrat, M.S., Nieuwenhuis, S., Jepma, M., and Cohen, J.D. (2010). Pupil diameter tracks changes in control state predicted by the adaptive gain theory of locus coeruleus function. Cogn Affect Behav Neurosci *10*, 252-269. 10.3758/CABN.10.2.252.

Goadsby, P.J., Lambert, G.A., and Lance, J.W. (1985). The mechanism of cerebrovascular vasoconstriction in response to locus coeruleus stimulation. Brain Res *326*, 213-217. 10.1016/0006-8993(85)90030-7.

Golan, T., Davidesco, I., Meshulam, M., Groppe, D.M., Megevand, P., Yeagle, E.M., Goldfinger, M.S., Harel, M., Melloni, L., Schroeder, C.E., et al. (2016). Human intracranial recordings link suppressed transients rather than 'filling-in' to perceptual continuity across blinks. Elife *5*. 10.7554/eLife.17243.

Gray, S.R., Ye, L., Ye, J.Y., and Paukert, M. (2021). Noradrenergic terminal short-term potentiation enables modality-selective integration of sensory input and vigilance state. Sci Adv *7*, eabk1378. 10.1126/sciadv.abk1378.

Guipponi, O., Odouard, S., Pinede, S., Wardak, C., and Ben Hamed, S. (2015). fMRI Cortical Correlates of Spontaneous Eye Blinks in the Nonhuman Primate. Cereb Cortex *25*, 2333-2345. 10.1093/cercor/bhu038.

Hakerem, G., and Sutton, S. (1966). Pupillary response at visual threshold. Nature *212*, 485-486. 10.1038/212485a0.

Hayat, H., Regev, N., Matosevich, N., Sales, A., Paredes-Rodriguez, E., Krom, A.J., Bergman, L., Li, Y., Lavigne, M., Kremer, E.J., et al. (2020). Locus coeruleus norepinephrine activity mediates sensory-evoked awakenings from sleep. Sci Adv *6*, eaaz4232. 10.1126/sciadv.aaz4232.

Hess, E.H., and Polt, J.M. (1964). Pupil Size in Relation to Mental Activity during Simple Problem-Solving. Science *143*, 1190-1192. 10.1126/science.143.3611.1190.

Holland, M.K., and Tarlow, G. (1972). Blinking and mental load. Psychol Rep *31*, 119-127. 10.2466/pr0.1972.31.1.119.

Huo, B.X., Gao, Y.R., and Drew, P.J. (2015). Quantitative separation of arterial and venous cerebral blood volume increases during voluntary locomotion. Neuroimage *105*, 369-379. 10.1016/j.neuroimage.2014.10.030.

Huo, B.X., Smith, J.B., and Drew, P.J. (2014). Neurovascular coupling and decoupling in the cortex during voluntary locomotion. J Neurosci *34*, 10975-10981. 10.1523/JNEUROSCI.1369-14.2014.

Hupe, J.M., Bordier, C., and Dojat, M. (2012). A BOLD signature of eyeblinks in the visual cortex. Neuroimage *61*, 149-161. 10.1016/j.neuroimage.2012.03.001.

Joshi, S., Li, Y., Kalwani, R.M., and Gold, J.I. (2016). Relationships between Pupil Diameter and Neuronal Activity in the Locus Coeruleus, Colliculi, and Cingulate Cortex. Neuron *89*, 221-234. 10.1016/j.neuron.2015.11.028.

Kahneman, D., and Beatty, J. (1966). Pupil diameter and load on memory. Science *154*, 1583-1585. 10.1126/science.154.3756.1583.

Kaminer, J., Powers, A.S., Horn, K.G., Hui, C., and Evinger, C. (2011). Characterizing the spontaneous blink generator: an animal model. J Neurosci *31*, 11256-11267. 10.1523/JNEUROSCI.6218-10.2011.

Karimi Abadchi, J., Nazari-Ahangarkolaee, M., Gattas, S., Bermudez-Contreras, E., Luczak, A., McNaughton, B.L., and Mohajerani, M.H. (2020). Spatiotemporal patterns of neocortical activity around hippocampal sharp-wave ripples. Elife *9*. 10.7554/eLife.51972.

Karson, C.N. (1979). Oculomotor signs in a psychiatric population: a preliminary report. Am J Psychiatry *136*, 1057-1060. 10.1176/ajp.136.8.1057.

Karson, C.N. (1983). Spontaneous eye-blink rates and dopaminergic systems. Brain *106 (Pt 3)*, 643-653. 10.1093/brain/106.3.643.

Karson, C.N., Dykman, R.A., and Paige, S.R. (1990). Blink rates in schizophrenia. Schizophr Bull *16*, 345-354. 10.1093/schbul/16.2.345.

Kjaerby, C., Andersen, M., Hauglund, N., Ding, F., Wang, W., Xu, Q., Deng, S., Kang, N., Peng, S., Sun, Q., et al. (2020). Dynamic fluctuations of the locus coeruleus-norepinephrine system underlie sleep state transitions. bioxriv pre-print. 10.1101/2020.09.01.274977.

Larsen, R.S., and Waters, J. (2018). Neuromodulatory Correlates of Pupil Dilation. Front Neural Circuits *12*, 21. 10.3389/fncir.2018.00021.

Le Van Quyen, M., Staba, R., Bragin, A., Dickson, C., Valderrama, M., Fried, I., and Engel, J. (2010). Large-scale microelectrode recordings of high-frequency gamma oscillations in human cortex during sleep. J Neurosci *30*, 7770-7782. 10.1523/JNEUROSCI.5049-09.2010.

Liu, X., de Zwart, J.A., Scholvinck, M.L., Chang, C., Ye, F.Q., Leopold, D.A., and Duyn, J.H. (2018). Subcortical evidence for a contribution of arousal to fMRI studies of brain activity. Nat Commun *9*, 395. 10.1038/s41467-017-02815-3.

Liu, X., Yanagawa, T., Leopold, D.A., Chang, C., Ishida, H., Fujii, N., and Duyn, J.H. (2015). Arousal transitions in sleep, wakefulness, and anesthesia are characterized by an orderly sequence of cortical events. Neuroimage *116*, 222-231. 10.1016/j.neuroimage.2015.04.003.

Longden, T.A., Dabertrand, F., Koide, M., Gonzales, A.L., Tykocki, N.R., Brayden, J.E., Hill-Eubanks, D., and Nelson, M.T. (2017). Capillary K(+)-sensing initiates retrograde hyperpolarization to increase local cerebral blood flow. Nat Neurosci *20*, 717-726. 10.1038/nn.4533.

Ma, Y., Shaik, M.A., Kim, S.H., Kozberg, M.G., Thibodeaux, D.N., Zhao, H.T., Yu, H., and Hillman, E.M. (2016a). Wide-field optical mapping of neural activity and brain haemodynamics: considerations and novel approaches. Philos Trans R Soc Lond B Biol Sci *371*. 10.1098/rstb.2015.0360.

Ma, Y., Shaik, M.A., Kozberg, M.G., Kim, S.H., Portes, J.P., Timerman, D., and Hillman, E.M. (2016b). Resting-state hemodynamics are spatiotemporally coupled to synchronized and symmetric neural activity in excitatory neurons. Proc Natl Acad Sci U S A *113*, E8463-E8471. 10.1073/pnas.1525369113.

McGinley, M.J., David, S.V., and McCormick, D.A. (2015). Cortical Membrane Potential Signature of Optimal States for Sensory Signal Detection. Neuron *87*, 179-192. 10.1016/j.neuron.2015.05.038.

Megemont, M., McBurney-Lin, J., and Yang, H. (2022). Pupil diameter is not an accurate real-time readout of locus coeruleus activity. Elife *11*. 10.7554/eLife.70510.

Montgomery, S.M., Sirota, A., and Buzsaki, G. (2008). Theta and gamma coordination of hippocampal networks during waking and rapid eye movement sleep. J Neurosci *28*, 6731-6741. 10.1523/JNEUROSCI.1227-08.2008.

Morad, Y., Lemberg, H., Yofe, N., and Dagan, Y. (2000). Pupillography as an objective indicator of fatigue. Curr Eye Res *21*, 535-542.

Murphy, P.R., O'Connell, R.G., O'Sullivan, M., Robertson, I.H., and Balsters, J.H. (2014). Pupil diameter covaries with BOLD activity in human locus coeruleus. Hum Brain Mapp *35*, 4140-4154. 10.1002/hbm.22466.

Musall, S., Kaufman, M.T., Juavinett, A.L., Gluf, S., and Churchland, A.K. (2019). Single-trial neural dynamics are dominated by richly varied movements. Nat Neurosci *22*, 1677-1686. 10.1038/s41593-019-0502-4.

Nakamori, K., Odawara, M., Nakajima, T., Mizutani, T., and Tsubota, K. (1997). Blinking is controlled primarily by ocular surface conditions. American Journal of Ophthalmology *124*, 24-30. Doi 10.1016/S0002-9394(14)71639-3.

Nakano, T., Kato, M., Morito, Y., Itoi, S., and Kitazawa, S. (2013). Blink-related momentary activation of the default mode network while viewing videos. Proc Natl Acad Sci U S A *110*, 702-706. 10.1073/pnas.1214804110.

Nassar, M.R., Rumsey, K.M., Wilson, R.C., Parikh, K., Heasly, B., and Gold, J.I. (2012). Rational regulation of learning dynamics by pupil-linked arousal systems. Nat Neurosci *15*, 1040-1046. 10.1038/nn.3130.

Onorati, F., Barbieri, R., Mauri, M., Russo, V., and Mainardi, L. (2013). Characterization of affective states by pupillary dynamics and autonomic correlates. Front Neuroeng *6*, 9. 10.3389/fneng.2013.00009.

Osorio-Forero, A., Cardis, R., Vantomme, G., Guillaume-Gentil, A., Katsioudi, G., Devenoges, C., Fernandez, L.M.J., and Luthi, A. (2021). Noradrenergic circuit control of non-REM sleep substates. Curr Biol *31*, 5009-5023 e5007. 10.1016/j.cub.2021.09.041.

Pais-Roldan, P., Takahashi, K., Sobczak, F., Chen, Y., Zhao, X., Zeng, H., Jiang, Y., and Yu, X. (2020). Indexing brain state-dependent pupil dynamics with simultaneous fMRI and optical fiber calcium recording. Proc Natl Acad Sci U S A *117*, 6875-6882. 10.1073/pnas.1909937117.

Paukert, M., Agarwal, A., Cha, J., Doze, V.A., Kang, J.U., and Bergles, D.E. (2014). Norepinephrine controls astroglial responsiveness to local circuit activity. Neuron *82*, 1263-1270. 10.1016/j.neuron.2014.04.038.

Petersen, C.C. (2007). The functional organization of the barrel cortex. Neuron *56*, 339-355. 10.1016/j.neuron.2007.09.017.

Petersen, C.C. (2014). Cortical control of whisker movement. Annu Rev Neurosci *37*, 183-203. 10.1146/annurev-neuro-062012-170344.

Polack, P.O., Friedman, J., and Golshani, P. (2013). Cellular mechanisms of brain state-dependent gain modulation in visual cortex. Nat Neurosci *16*, 1331-1339. 10.1038/nn.3464.

Preuschoff, K., t Hart, B.M., and Einhauser, W. (2011). Pupil Dilation Signals Surprise: Evidence for Noradrenaline's Role in Decision Making. Front Neurosci *5*, 115. 10.3389/fnins.2011.00115.

Raichle, M.E., Hartman, B.K., Eichling, J.O., and Sharpe, L.G. (1975). Central noradrenergic regulation of cerebral blood flow and vascular permeability. Proc Natl Acad Sci U S A *72*, 3726-3730. 10.1073/pnas.72.9.3726.

Rasmussen, R., Nicholas, E., Petersen, N.C., Dietz, A.G., Xu, Q., Sun, Q., and Nedergaard, M. (2019). Cortex-wide Changes in Extracellular Potassium Ions Parallel Brain State Transitions in Awake Behaving Mice. Cell Rep *28*, 1182-1194 e1184. 10.1016/j.celrep.2019.06.082.

Reimer, J., Froudarakis, E., Cadwell, C.R., Yatsenko, D., Denfield, G.H., and Tolias, A.S. (2014). Pupil fluctuations track fast switching of cortical states during quiet wakefulness. Neuron *84*, 355-362. 10.1016/j.neuron.2014.09.033.

Reimer, J., McGinley, M.J., Liu, Y., Rodenkirch, C., Wang, Q., McCormick, D.A., and Tolias, A.S. (2016). Pupil fluctuations track rapid changes in adrenergic and cholinergic activity in cortex. Nat Commun *7*, 13289. 10.1038/ncomms13289.

Salkoff, D.B., Zagha, E., McCarthy, E., and McCormick, D.A. (2020). Movement and Performance Explain Widespread Cortical Activity in a Visual Detection Task. Cereb Cortex *30*, 421-437. 10.1093/cercor/bhz206.

Saper, C.B., and Fuller, P.M. (2017). Wake-sleep circuitry: an overview. Curr Opin Neurobiol *44*, 186-192. 10.1016/j.conb.2017.03.021.

Schwarz, L.A., and Luo, L. (2015). Organization of the locus coeruleus-norepinephrine system. Curr Biol *25*, R1051-R1056. 10.1016/j.cub.2015.09.039.

Shih, A.Y., Mateo, C., Drew, P.J., Tsai, P.S., and Kleinfeld, D. (2012). A polished and reinforced thinned-skull window for long-term imaging of the mouse brain. J Vis Exp. 10.3791/3742.

Sirotin, Y.B., and Das, A. (2009). Anticipatory haemodynamic signals in sensory cortex not predicted by local neuronal activity. Nature *457*, 475-479. 10.1038/nature07664.

Sobczak, F., Pais-Roldan, P., Takahashi, K., and Yu, X. (2021). Decoding the brain state-dependent relationship between pupil dynamics and resting state fMRI signal fluctuation. Elife *10*. 10.7554/eLife.68980.

Steriade, M., Nunez, A., and Amzica, F. (1993). A novel slow (< 1 Hz) oscillation of neocortical neurons in vivo: depolarizing and hyperpolarizing components. The Journal of Neuroscience *13*, 3252-3265. 10.1523/jneurosci.13-08-03252.1993.

Stern, J.A., Boyer, D., and Schroeder, D. (1994). Blink rate: a possible measure of fatigue. Hum Factors *36*, 285-297. 10.1177/001872089403600209.

Stern, J.A., Walrath, L.C., and Goldstein, R. (1984). The endogenous eyeblink. Psychophysiology *21*, 22-33. 10.1111/j.1469-8986.1984.tb02312.x.

Strauch, C., Wang, C.A., Einhauser, W., Van der Stigchel, S., and Naber, M. (2022). Pupillometry as an integrated readout of distinct attentional networks. Trends Neurosci. 10.1016/j.tins.2022.05.003.

Stringer, C., Pachitariu, M., Steinmetz, N., Reddy, C.B., Carandini, M., and Harris, K.D. (2019). Spontaneous behaviors drive multidimensional, brainwide activity. Science *364*, 255. 10.1126/science.aav7893.

Sullivan, D., Mizuseki, K., Sorgi, A., and Buzsaki, G. (2014). Comparison of sleep spindles and theta oscillations in the hippocampus. J Neurosci *34*, 662-674. 10.1523/JNEUROSCI.0552-13.2014.

Tagliazucchi, E., and Laufs, H. (2014). Decoding wakefulness levels from typical fMRI resting-state data reveals reliable drifts between wakefulness and sleep. Neuron *82*, 695-708. 10.1016/j.neuron.2014.03.020.

Toussay, X., Basu, K., Lacoste, B., and Hamel, E. (2013). Locus coeruleus stimulation recruits a broad cortical neuronal network and increases cortical perfusion. J Neurosci *33*, 3390-3401. 10.1523/JNEUROSCI.3346-12.2013.

Turner, K.L., Gheres, K.W., Proctor, E.A., and Drew, P.J. (2020). Neurovascular coupling and bilateral connectivity during NREM and REM sleep. Elife *9*. 10.7554/eLife.62071.

Van Orden, K.F., Limbert, W., Makeig, S., and Jung, T.P. (2001). Eye activity correlates of workload during a visuospatial memory task. Hum Factors *43*, 111-121. 10.1518/001872001775992570.

Vazquez, A.L., Fukuda, M., Crowley, J.C., and Kim, S.G. (2014). Neural and hemodynamic responses elicited by forelimb- and photo-stimulation in channelrhodopsin-2 mice: insights into the hemodynamic point spread function. Cereb Cortex *24*, 2908-2919. 10.1093/cercor/bht147.

Vinck, M., Batista-Brito, R., Knoblich, U., and Cardin, J.A. (2015). Arousal and locomotion make distinct contributions to cortical activity patterns and visual encoding. Neuron *86*, 740-754. 10.1016/j.neuron.2015.03.028.

Weber, F., and Dan, Y. (2016). Circuit-based interrogation of sleep control. Nature *538*, 51-59. 10.1038/nature19773.

Winder, A.T., Echagarruga, C., Zhang, Q., and Drew, P.J. (2017). Weak correlations between hemodynamic signals and ongoing neural activity during the resting state. Nat Neurosci *20*, 1761-1769. 10.1038/s41593-017-0007-y.

Yang, H., Bari, B.A., Cohen, J.Y., and O'Connor, D.H. (2021). Locus coeruleus spiking differently correlates with S1 cortex activity and pupil diameter in a tactile detection task. Elife *10*. 10.7554/eLife.64327.

Yoss, R.E., Moyer, N.J., and Hollenhorst, R.W. (1970). Pupil size and spontaneous pupillary waves associated with alertness, drowsiness, and sleep. Neurology *20*, 545-554. 10.1212/wnl.20.6.545.

Yuzgec, O., Prsa, M., Zimmermann, R., and Huber, D. (2018). Pupil Size Coupling to Cortical States Protects the Stability of Deep Sleep via Parasympathetic Modulation. Curr Biol *28*, 392-400 e393. 10.1016/j.cub.2017.12.049.

Zhang, Q., Cramer, S.R., Ma, Z., Turner, K.L., Gheres, K.W., Liu, Y., Drew, P.J., and Zhang, N. (2022a). Brain-wide ongoing activity is responsible for significant cross-trial BOLD variability. Cereb Cortex. 10.1093/cercor/bhac016.

Zhang, Q., Roche, M., Gheres, K.W., Chaigneau, E., Kedarasetti, R.T., Haselden, W.D., Charpak, S., and Drew, P.J. (2019). Cerebral oxygenation during locomotion is modulated by respiration. Nat Commun *10*, 5515. 10.1038/s41467-019-13523-5.

Zhang, Q., Turner, K.L., Gheres, K.W., Hossain, M.S., and Drew, P.J. (2022b). Behavioral and physiological monitoring for awake neurovascular coupling experiments: a how-to guide. Neurophotonics *9*, 021905. 10.1117/1.NPh.9.2.021905.

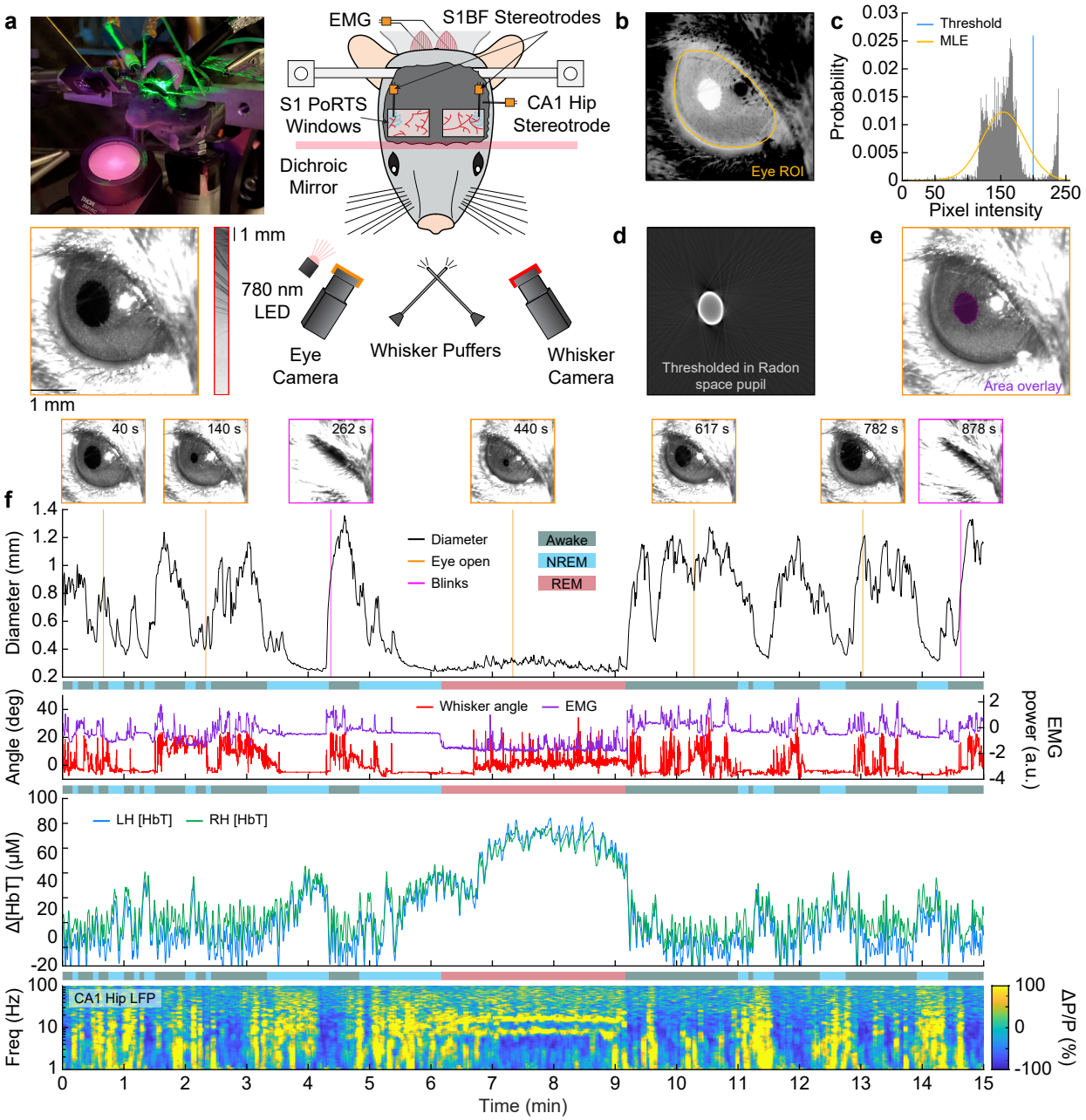
a
EMG
S1BF Stereotrodes
S1 PoRTS Windows
CA1 Hip Stereotrode
Dichroic Mirror
1 mm
780 nm LED
Eye Camera
Whisker Puffers
Whisker Camera
1 mm
b
Eye ROI
c
Threshold
MLE
Probability
Pixel intensity
d
Thresholded in Radon space pupil
e
Area overlay
40 s
140 s
262 s
440 s
617 s
782 s
878 s
f
Diameter (mm)
Diameter
Eye open
Blinks
Awake
NREM
REM
Angle (deg)
Whisker angle
EMG
EMG power (a.u.)
Δ[HbT] (μM)
LH [HbT]
RH [HbT]
Freq (Hz)
CA1 Hip LFP
ΔP/P (%)
Time (min)

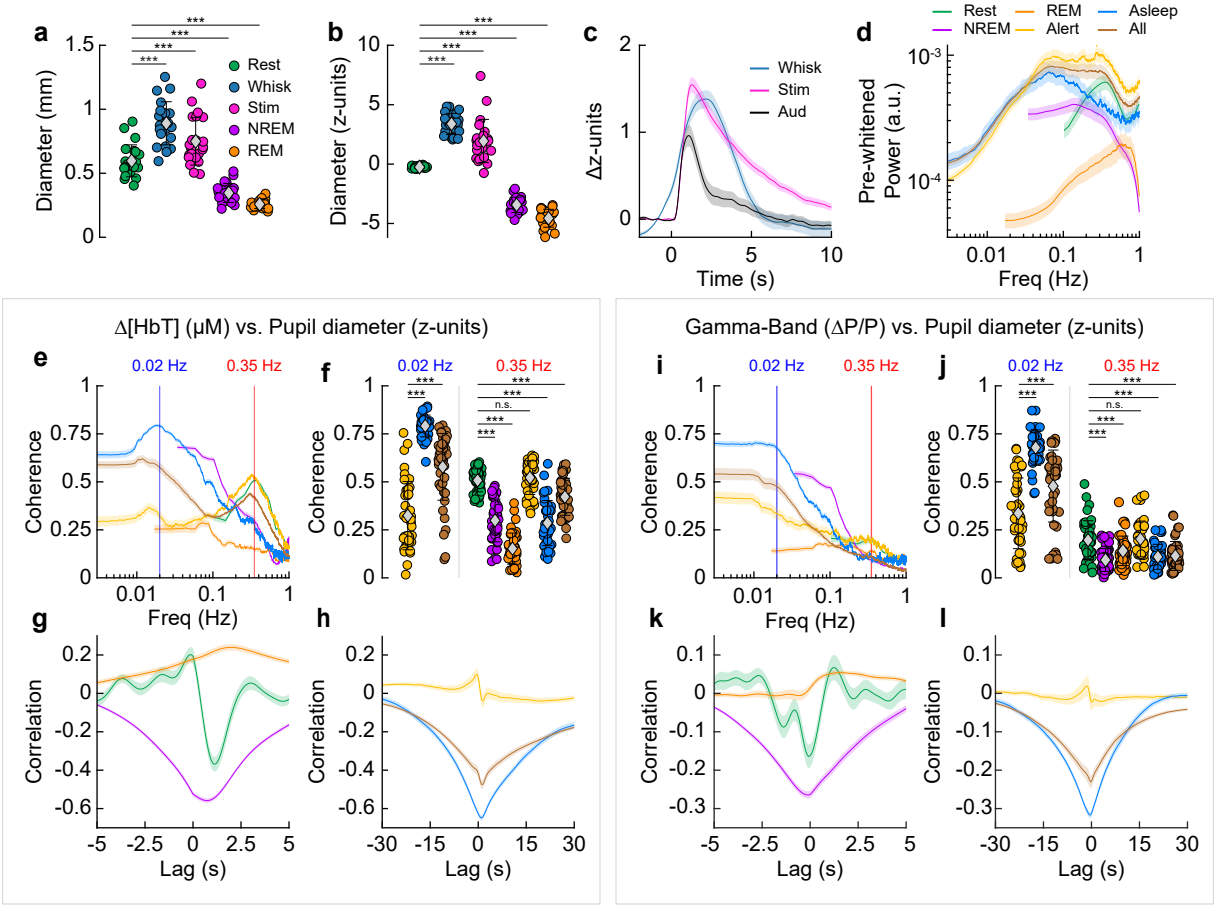
a
Diameter (mm)
Rest
Whisk
Stim
NREM
REM
b
Diameter (z-units)
c
Δz-units
Whisk
Stim
Aud
Time (s)
d
Pre-whitened Power (a.u.)
Rest
NREM
REM
Alert
Asleep
All
Freq (Hz)
Δ[HbT] (μM) vs. Pupil diameter (z-units)
e
0.02 Hz
0.35 Hz
Coherence
Freq (Hz)
f
Coherence
n.s.
g
Correlation
Lag (s)
h
Correlation
Lag (s)
Gamma-Band (ΔP/P) vs. Pupil diameter (z-units)
i
0.02 Hz
0.35 Hz
Coherence
Freq (Hz)
j
Coherence
n.s.
k
Correlation
Lag (s)
l
Correlation
Lag (s)

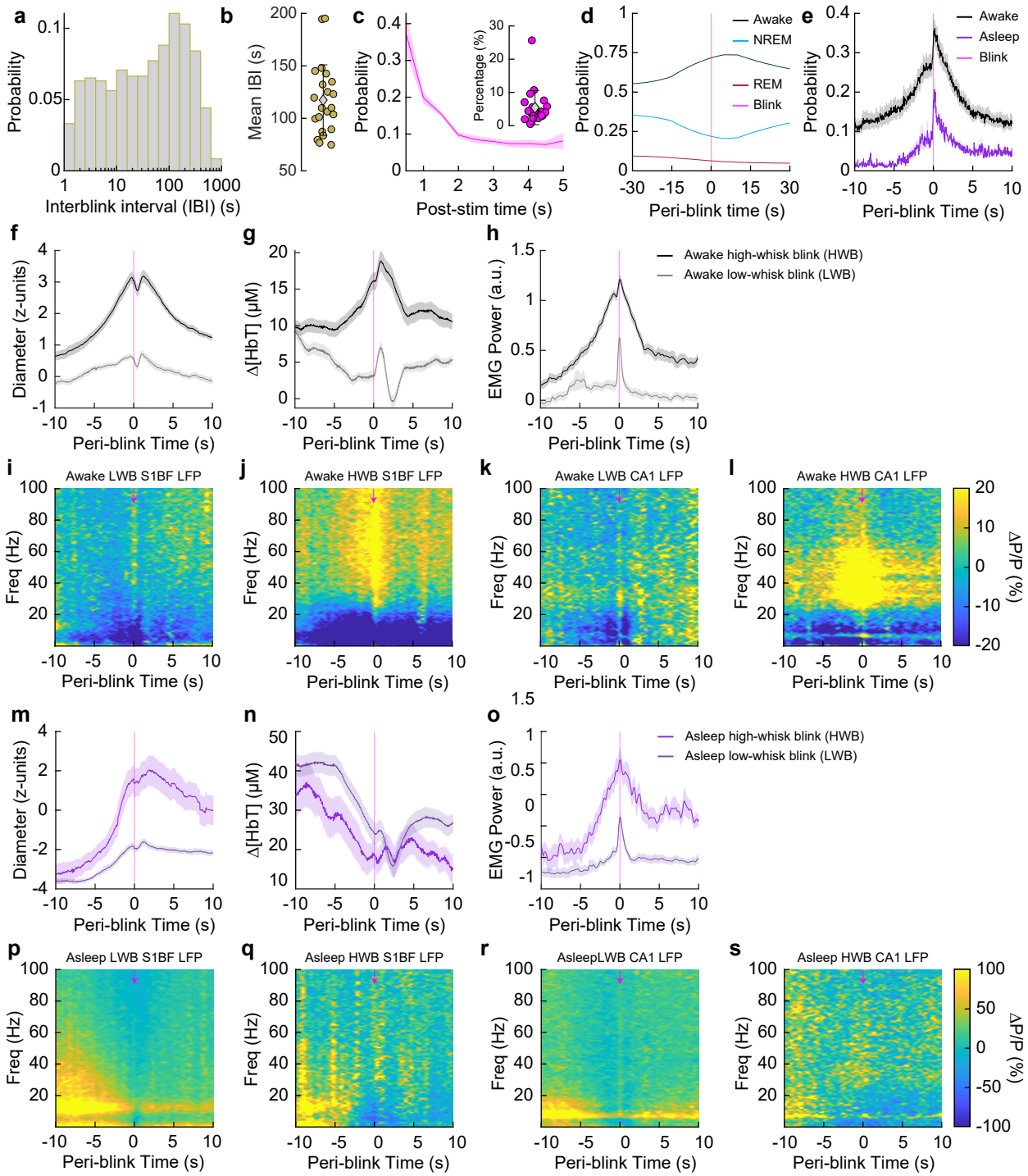
a
Probability
Interblink interval (IBI) (s)
b
Mean IBI (s)
c
Probability
Post-stim time (s)
Percentage (%)
d
Probability
Peri-blink time (s)
Awake
NREM
REM
Blink
e
Probability
Peri-blink Time (s)
Awake
Asleep
Blink
f
Diameter (z-units)
Peri-blink Time (s)
g
Δ[HbT] (μM)
Peri-blink Time (s)
h
EMG Power (a.u.)
Peri-blink Time (s)
Awake high-whisk blink (HWB)
Awake low-whisk blink (LWB)
i
Awake LWB S1BF LFP
Freq (Hz)
Peri-blink Time (s)
j
Awake HWB S1BF LFP
Freq (Hz)
Peri-blink Time (s)
k
Awake LWB CA1 LFP
Freq (Hz)
Peri-blink Time (s)
l
Awake HWB CA1 LFP
Freq (Hz)
Peri-blink Time (s)
ΔP/P (%)
m
Diameter (z-units)
Peri-blink Time (s)
n
Δ[HbT] (μM)
Peri-blink Time (s)
o
EMG Power (a.u.)
Peri-blink Time (s)
Asleep high-whisk blink (HWB)
Asleep low-whisk blink (LWB)
p
Asleep LWB S1BF LFP
Freq (Hz)
Peri-blink Time (s)
q
Asleep HWB S1BF LFP
Freq (Hz)
Peri-blink Time (s)
r
AsleepLWB CA1 LFP
Freq (Hz)
Peri-blink Time (s)
s
Asleep HWB CA1 LFP
Freq (Hz)
Peri-blink Time (s)
ΔP/P (%)

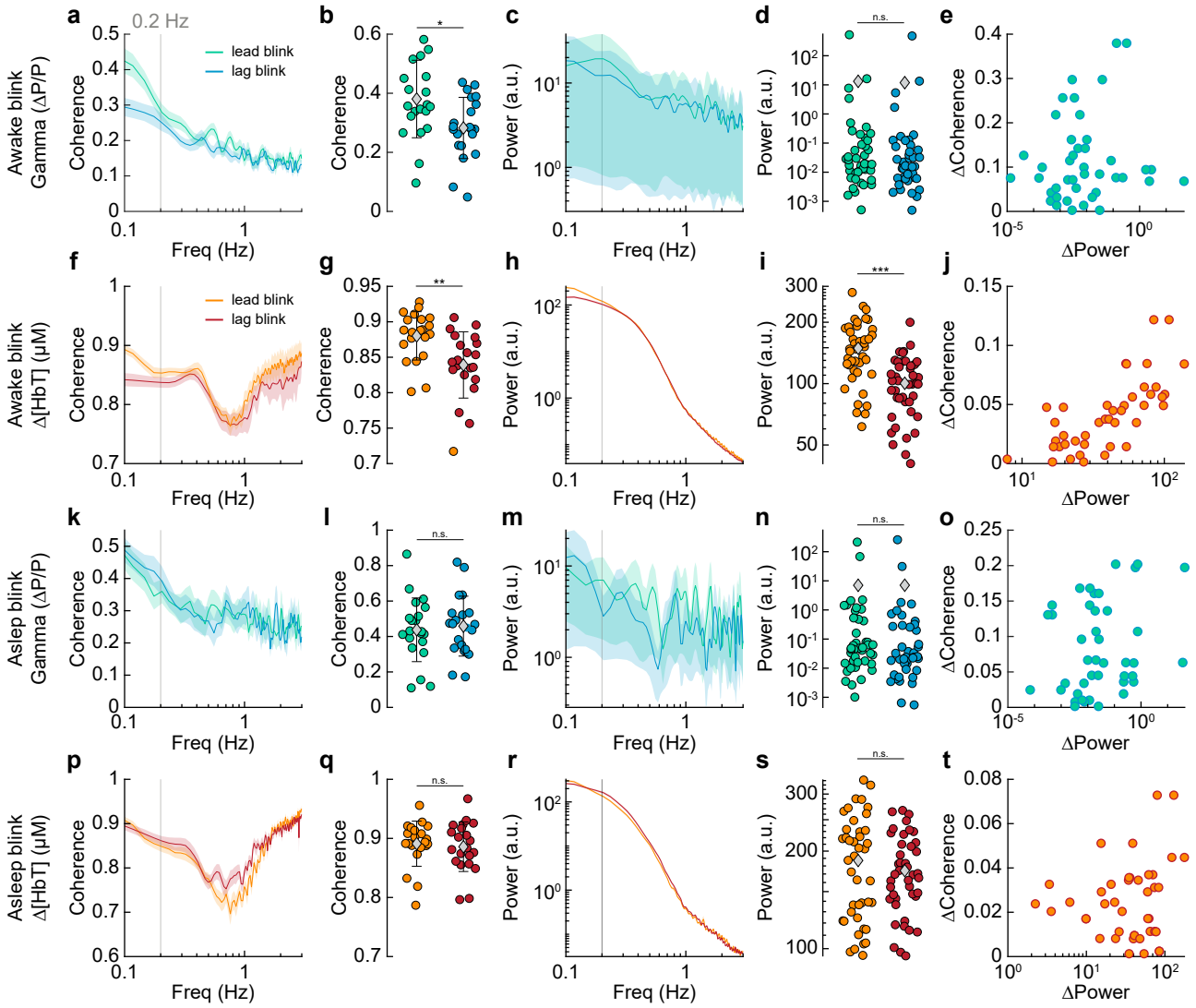
a
0.2 Hz
lead blink
lag blink
Awake blink
Gamma (ΔP/P)
Coherence
Freq (Hz)
b
Coherence
*
c
Power (a.u.)
Freq (Hz)
d
Power (a.u.)
n.s.
e
ΔCoherence
ΔPower
f
lead blink
lag blink
Awake blink
Δ[HbT] (μM)
Coherence
Freq (Hz)
g
Coherence
**
h
Power (a.u.)
Freq (Hz)
i
Power (a.u.)
***
j
ΔCoherence
ΔPower
k
Aslep blink
Gamma (ΔP/P)
Coherence
Freq (Hz)
l
Coherence
n.s.
m
Power (a.u.)
Freq (Hz)
n
Power (a.u.)
n.s.
o
ΔCoherence
ΔPower
p
Asleep blink
Δ[HbT] (μM)
Coherence
Freq (Hz)
q
Coherence
n.s.
r
Power (a.u.)
Freq (Hz)
s
Power (a.u.)
n.s.
t
ΔCoherence
ΔPower

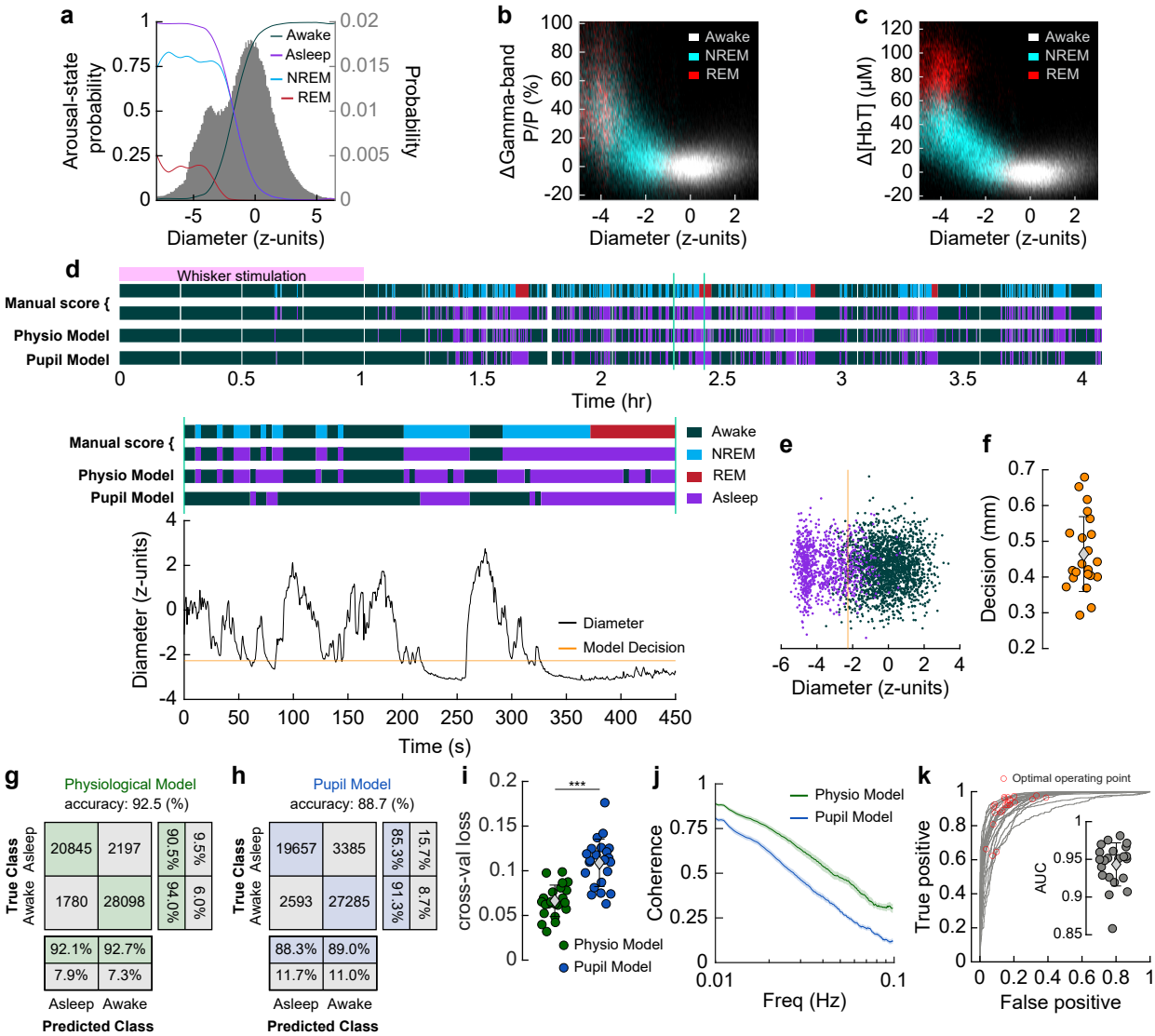
a
Arousal-state probability
Probability
Awake
Asleep
NREM
REM
Diameter (z-units)
b
ΔGamma-band P/P (%)
Awake
NREM
REM
Diameter (z-units)
c
Δ[HbT] (μM)
Awake
NREM
REM
Diameter (z-units)
d
Whisker stimulation
Manual score {
Physio Model
Pupil Model
Time (hr)
Manual score {
Physio Model
Pupil Model
Awake
NREM
REM
Asleep
Diameter (z-units)
Diameter
Model Decision
Time (s)
e
Diameter (z-units)
f
Decision (mm)
g
Physiological Model
accuracy: 92.5 (%)
True Class
Asleep
Awake
20845
2197
1780
28098
90.5%
9.5%
94.0%
6.0%
92.1%
92.7%
7.9%
7.3%
Asleep
Awake
Predicted Class
h
Pupil Model
accuracy: 88.7 (%)
True Class
Asleep
Awake
19657
3385
2593
27285
85.3%
15.7%
91.3%
8.7%
88.3%
89.0%
11.7%
11.0%
Asleep
Awake
Predicted Class
i
cross-val loss
***
Physio Model
Pupil Model
j
Coherence
Physio Model
Pupil Model
Freq (Hz)
k
Optimal operating point
True positive
AUC
False positive